Study of $\gamma\gamma \to \gamma\psi(2S)$ at Belle

X. L. Wang,[11] B. S. Gao,[11] W. J. Zhu,[11] I. Adachi,[19,15] H. Aihara,[91] S. Al Said,[84,39] D. M. Asner,[3] H. Atmacan,[7] V. Aulchenko,[4,68] T. Aushev,[21] R. Ayad,[84] V. Babu,[8] S. Bahinipati,[25] P. Behera,[28] V. Bhardwaj,[24] B. Bhuyan,[26] T. Bilka,[5] J. Biswal,[35] A. Bobrov,[4,68] G. Bonvicini,[94] A. Bozek,[64] M. Bračko,[51,35] M. Campajola,[33,59] D. Červenkov,[5] M.-C. Chang,[10] V. Chekelian,[52] A. Chen,[61] B. G. Cheon,[17] K. Chilikin,[46] H. E. Cho,[17] K. Cho,[41] S.-K. Choi,[16] Y. Choi,[82] S. Choudhury,[27] D. Cinabro,[94] S. Cunliffe,[8] S. Das,[50] G. De Nardo,[33,59] R. Dhamija,[27] F. Di Capua,[33,59] Z. Doležal,[5] T. V. Dong,[11] S. Eidelman,[4,68,46] T. Ferber,[8] D. Ferlewicz,[53] A. Frey,[14] B. G. Fulsom,[70] R. Garg,[71] V. Gaur,[93] N. Gabyshev,[4,68] A. Garmash,[4,68] A. Giri,[27] P. Goldenzweig,[36] B. Golob,[47,35] C. Hadjivasiliou,[70] T. Hara,[19,15] O. Hartbrich,[18] K. Hayasaka,[66] H. Hayashii,[60] M. T. Hedges,[18] W.-S. Hou,[63] C.-L. Hsu,[83] T. Iijima,[58,57] K. Inami,[57] A. Ishikawa,[19,15] R. Itoh,[19,15] M. Iwasaki,[69] Y. Iwasaki,[19] W. W. Jacobs,[29] S. Jia,[11] Y. Jin,[91] C. W. Joo,[37] K. K. Joo,[6] J. Kahn,[36] K. H. Kang,[44] T. Kawasaki,[40] C. Kiesling,[52] C. H. Kim,[17] D. Y. Kim,[81] S. H. Kim,[78] Y.-K. Kim,[96] P. Kodyš,[5] T. Konno,[40] A. Korobov,[4,68] S. Korpar,[51,35] E. Kovalenko,[4,68] P. Križan,[47,35] R. Kroeger,[54] P. Krokovny,[4,68] R. Kulasiri,[38] M. Kumar,[50] R. Kumar,[74] K. Kumara,[94] A. Kuzmin,[4,68] Y.-J. Kwon,[96] K. Lalwani,[50] J. S. Lange,[12] I. S. Lee,[17] S. C. Lee,[44] P. Lewis,[2] J. Li,[44] L. K. Li,[7] Y. B. Li,[72] L. Li Gioi,[52] J. Libby,[28] K. Lieret,[48] D. Liventsev,[94,19] C. MacQueen,[53] M. Masuda,[90,75] T. Matsuda,[55] D. Matvienko,[4,68,46] M. Merola,[33,59] F. Metzner,[36] K. Miyabayashi,[60] R. Mizuk,[46,21] G. B. Mohanty,[85] M. Mrvar,[32] R. Mussa,[34] M. Nakao,[19,15] Z. Natkaniec,[64] A. Natochii,[18] L. Nayak,[27] M. Nayak,[87] M. Niiyama,[43] N. K. Nisar,[3] S. Nishida,[19,15] K. Nishimura,[18] S. Ogawa,[88] H. Ono,[65,66] Y. Onuki,[91] P. Oskin,[46] P. Pakhlov,[46,56] G. Pakhlova,[21,46] T. Pang,[73] S. Pardi,[33] H. Park,[44] S.-H. Park,[19] S. Patra,[24] S. Paul,[86,52] T. K. Pedlar,[49] R. Pestotnik,[35] L. E. Piilonen,[93] T. Podobnik,[47,35] V. Popov,[21] E. Prencipe,[22] M. T. Prim,[2] M. Röhrken,[8] A. Rostomyan,[8] N. Rout,[28] G. Russo,[59] D. Sahoo,[85] S. Sandilya,[27] A. Sangal,[7] L. Santelj,[47,35] T. Sanuki,[89] G. Schnell,[1,23] C. Schwanda,[32] Y. Seino,[66] K. Senyo,[95] M. E. Sevior,[53] M. Shapkin,[31] C. Sharma,[50] C. P. Shen,[11] J.-G. Shiu,[63] B. Shwartz,[4,68] F. Simon,[52] J. B. Singh,[71] A. Sokolov,[31] E. Solovieva,[46] S. Stanič,[67] M. Starič,[35] Z. S. Stottler,[93] M. Sumihama,[13] M. Takizawa,[79,20,76] U. Tamponi,[34] F. Tenchini,[8] M. Uchida,[92] S. Uehara,[19,15] T. Uglov,[46,21] Y. Unno,[17] S. Uno,[19,15] P. Urquijo,[53] Y. Usov,[4,68] R. Van Tonder,[2] G. Varner,[18] A. Vossen,[9] E. Waheed,[19] C. H. Wang,[62] M.-Z. Wang,[63] P. Wang,[30] M. Watanabe,[66] S. Watanuki,[45] O. Werbycka,[64] E. Won,[42] X. Xu,[80] W. Yan,[77] S. B. Yang,[42] H. Ye,[8] J. H. Yin,[42] C. Z. Yuan,[30] Z. P. Zhang,[77] V. Zhilich,[4,68] and V. Zhukova[46]

(Belle Collaboration)

[1]*Department of Physics, University of the Basque Country UPV/EHU, 48080 Bilbao, Spain*
[2]*University of Bonn, 53115 Bonn, Germany*
[3]*Brookhaven National Laboratory, Upton, New York 11973, USA*
[4]*Budker Institute of Nuclear Physics SB RAS, Novosibirsk 630090, Russian Federation*
[5]*Faculty of Mathematics and Physics, Charles University, 121 16 Prague, The Czech Republic*
[6]*Chonnam National University, Gwangju 61186, South Korea*
[7]*University of Cincinnati, Cincinnati, Ohio 45221, USA*
[8]*Deutsches Elektronen–Synchrotron, 22607 Hamburg, Germany*
[9]*Duke University, Durham, North Carolina 27708, USA*
[10]*Department of Physics, Fu Jen Catholic University, Taipei 24205, Taiwan*
[11]*Key Laboratory of Nuclear Physics and Ion-beam Application (MOE) and Institute of Modern Physics, Fudan University, Shanghai 200443, People's Republic of China*
[12]*Justus-Liebig-Universität Gießen, 35392 Gießen, Germany*
[13]*Gifu University, Gifu 501-1193, Japan*
[14]*II. Physikalisches Institut, Georg-August-Universität Göttingen, 37073 Göttingen, Germany*
[15]*SOKENDAI (The Graduate University for Advanced Studies), Hayama 240-0193, Japan*
[16]*Gyeongsang National University, Jinju 52828, South Korea*
[17]*Department of Physics and Institute of Natural Sciences, Hanyang University, Seoul 04763, South Korea*
[18]*University of Hawaii, Honolulu, Hawaii 96822, USA*
[19]*High Energy Accelerator Research Organization (KEK), Tsukuba 305-0801, Japan*
[20]*J-PARC Branch, KEK Theory Center, High Energy Accelerator Research Organization (KEK), Tsukuba 305-0801, Japan*
[21]*Higher School of Economics (HSE), Moscow 101000, Russian Federation*
[22]*Forschungszentrum Jülich, 52425 Jülich, Germany*
[23]*IKERBASQUE, Basque Foundation for Science, 48013 Bilbao, Spain*
[24]*Indian Institute of Science Education and Research Mohali, Sahibzada Ajit Singh Nagar, 140306, India*

[25]*Indian Institute of Technology Bhubaneswar, Bhubaneswar 752050, India*
[26]*Indian Institute of Technology Guwahati, Assam 781039, India*
[27]*Indian Institute of Technology Hyderabad, Telangana 502285, India*
[28]*Indian Institute of Technology Madras, Chennai 600036, India*
[29]*Indiana University, Bloomington, Indiana 47408, USA*
[30]*Institute of High Energy Physics, Chinese Academy of Sciences, Beijing 100049, People's Republic of China*
[31]*Institute for High Energy Physics, Protvino 142281, Russian Federation*
[32]*Institute of High Energy Physics, Vienna 1050, Austria*
[33]*INFN—Sezione di Napoli, 80126 Napoli, Italy*
[34]*INFN—Sezione di Torino, 10125 Torino, Italy*
[35]*J. Stefan Institute, 1000 Ljubljana, Slovenia*
[36]*Institut für Experimentelle Teilchenphysik, Karlsruher Institut für Technologie, 76131 Karlsruhe, Germany*
[37]*Kavli Institute for the Physics and Mathematics of the Universe (WPI), University of Tokyo, Kashiwa 277-8583, Japan*
[38]*Kennesaw State University, Kennesaw, Georgia 30144, USA*
[39]*Department of Physics, Faculty of Science, King Abdulaziz University, Jeddah 21589, Saudi Arabia*
[40]*Kitasato University, Sagamihara 252-0373, Japan*
[41]*Korea Institute of Science and Technology Information, Daejeon 34141, South Korea*
[42]*Korea University, Seoul 02841, South Korea*
[43]*Kyoto Sangyo University, Kyoto 603-8555, Japan*
[44]*Kyungpook National University, Daegu 41566, South Korea*
[45]*Université Paris-Saclay, CNRS/IN2P3, IJCLab, 91405 Orsay, France*
[46]*P.N. Lebedev Physical Institute of the Russian Academy of Sciences, Moscow 119991, Russian Federation*
[47]*Faculty of Mathematics and Physics, University of Ljubljana, 1000 Ljubljana, Slovenia*
[48]*Ludwig Maximilians University, 80539 Munich, Germany*
[49]*Luther College, Decorah, Iowa 52101, USA*
[50]*Malaviya National Institute of Technology Jaipur, Jaipur 302017, India*
[51]*Faculty of Chemistry and Chemical Engineering, University of Maribor, 2000 Maribor, Slovenia*
[52]*Max-Planck-Institut für Physik, 80805 München, Germany*
[53]*School of Physics, University of Melbourne, Victoria 3010, Australia*
[54]*University of Mississippi, University, Mississippi 38677, USA*
[55]*University of Miyazaki, Miyazaki 889-2192, Japan*
[56]*Moscow Physical Engineering Institute, Moscow 115409, Russian Federation*
[57]*Graduate School of Science, Nagoya University, Nagoya 464-8602, Japan*
[58]*Kobayashi-Maskawa Institute, Nagoya University, Nagoya 464-8602, Japan*
[59]*Università di Napoli Federico II, 80126 Napoli, Italy*
[60]*Nara Women's University, Nara 630-8506, Japan*
[61]*National Central University, Chung-li 32054, Taiwan*
[62]*National United University, Miao Li 36003, Taiwan*
[63]*Department of Physics, National Taiwan University, Taipei 10617, Taiwan*
[64]*H. Niewodniczanski Institute of Nuclear Physics, Krakow 31-342, Poland*
[65]*Nippon Dental University, Niigata 951-8580, Japan*
[66]*Niigata University, Niigata 950-2181, Japan*
[67]*University of Nova Gorica, 5000 Nova Gorica, Slovenia*
[68]*Novosibirsk State University, Novosibirsk 630090, Russian Federation*
[69]*Osaka City University, Osaka 558-8585, Japan*
[70]*Pacific Northwest National Laboratory, Richland, Washington 99352, USA*
[71]*Panjab University, Chandigarh 160014, India*
[72]*Peking University, Beijing 100871, People's Republic of China*
[73]*University of Pittsburgh, Pittsburgh, Pennsylvania 15260, USA*
[74]*Punjab Agricultural University, Ludhiana 141004, India*
[75]*Research Center for Nuclear Physics, Osaka University, Osaka 567-0047, Japan*
[76]*Meson Science Laboratory, Cluster for Pioneering Research, RIKEN, Saitama 351-0198, Japan*
[77]*Department of Modern Physics and State Key Laboratory of Particle Detection and Electronics, University of Science and Technology of China, Hefei 230026, People's Republic of China*
[78]*Seoul National University, Seoul 08826, South Korea*
[79]*Showa Pharmaceutical University, Tokyo 194-8543, Japan*

[80]Soochow University, Suzhou 215006, China
[81]Soongsil University, Seoul 06978, South Korea
[82]Sungkyunkwan University, Suwon 16419, South Korea
[83]School of Physics, University of Sydney, New South Wales 2006, Australia
[84]Department of Physics, Faculty of Science, University of Tabuk, Tabuk 71451, Saudi Arabia
[85]Tata Institute of Fundamental Research, Mumbai 400005, India
[86]Department of Physics, Technische Universität München, 85748 Garching, Germany
[87]School of Physics and Astronomy, Tel Aviv University, Tel Aviv 69978, Israel
[88]Toho University, Funabashi 274-8510, Japan
[89]Department of Physics, Tohoku University, Sendai 980-8578, Japan
[90]Earthquake Research Institute, University of Tokyo, Tokyo 113-0032, Japan
[91]Department of Physics, University of Tokyo, Tokyo 113-0033, Japan
[92]Tokyo Institute of Technology, Tokyo 152-8550, Japan
[93]Virginia Polytechnic Institute and State University, Blacksburg, Virginia 24061, USA
[94]Wayne State University, Detroit, Michigan 48202, USA
[95]Yamagata University, Yamagata 990-8560, Japan
[96]Yonsei University, Seoul 03722, South Korea

(Received 6 January 2022; accepted 15 June 2022; published 28 June 2022)

Using 980 fb^{-1} of data at and around the $\Upsilon(nS)$ ($n = 1, 2, 3, 4, 5$) resonances collected with the Belle detector at the KEKB asymmetric-energy e^+e^- collider, the two-photon process $\gamma\gamma \to \gamma\psi(2S)$ is studied from the threshold to 4.2 GeV for the first time. Two structures are seen in the invariant mass distribution of $\gamma\psi(2S)$: one at $M_{R_1} = 3922.4 \pm 6.5 \pm 2.0$ MeV/c^2 with a width of $\Gamma_{R_1} = 22 \pm 17 \pm 4$ MeV, and another at $M_{R_2} = 4014.3 \pm 4.0 \pm 1.5$ MeV/c^2 with a width of $\Gamma_{R_2} = 4 \pm 11 \pm 6$ MeV; the signals are parametrized with the incoherent sum of two Breit-Wigner functions. The first structure is consistent with the $X(3915)$ or the $\chi_{c2}(3930)$, and the local statistical significance is determined to be 3.1σ with the systematic uncertainties included. The second matches none of the known charmonium or charmoniumlike states, and its global significance is determined to be 2.8σ including the look-elsewhere effect. The production rates are $\Gamma_{\gamma\gamma}\mathcal{B}(R_1 \to \gamma\psi(2S)) = 9.8 \pm 3.6 \pm 1.3$ eV assuming $(J^{PC}, |\lambda|) = (0^{++}, 0)$ or $2.0 \pm 0.7 \pm 0.2$ eV with $(2^{++}, 2)$ for the first structure and $\Gamma_{\gamma\gamma}\mathcal{B}(R_2 \to \gamma\psi(2S)) = 6.2 \pm 2.2 \pm 0.8$ eV with $(0^{++}, 0)$ or $1.2 \pm 0.4 \pm 0.2$ eV with $(2^{++}, 2)$ for the second. Here, the first errors are statistical and the second systematic, and λ is the helicity.

DOI: 10.1103/PhysRevD.105.112011

I. INTRODUCTION

More than two dozen new resonances that are dubbed as X, Y and/or Z states have been found above the $D\bar{D}$ threshold since Belle observed the $X(3872)$ (now labeled the $\chi_{c1}(3872)$ [1]) in $B \to K\pi^+\pi^- J/\psi$ [2], and this number is much larger than the expectation from predictions of the conventional model. Among these, candidates for both conventional and exotic charmoniumlike states are discussed widely [3]. Many puzzles arise from these XYZ states, and one of them concerns the candidates for P-wave triplet states near 3.9 GeV/c^2, including the $X(3872)$, $Z(3930) \to D\bar{D}$ and $X(3915) \to \omega J/\psi$ observed in two-photon collisions [4–8], and $X^*(3860) \to D\bar{D}$ observed in a full amplitude analysis of the process $e^+e^- \to J/\psi D\bar{D}$ [9].

One of the most interesting XYZ states is the $X(3872)$, which lies very near the $D\bar{D}^* + \text{c.c.}$ mass threshold and is conjectured to have a large $D\bar{D}^* + \text{c.c.}$ molecular component [10]. Its large production rates in pp and $p\bar{p}$ collision experiments [11–14] and the determination of its quantum number by LHCb [15] suggest that there is a conventional charmonium $\chi_{c1}(2P)$ core in its wave function. This is supported by another study of $X(3872) \to \gamma\psi(2S)$ by LHCb [16]. A study of the line shape of this state by LHCb reveals a pole structure that is compatible with a quasibound state of $D^0\bar{D}^{*0}$ but allowing a quasivirtual state at the level of 2σ [17]. Partners of the $X(3872)$ are suggested, and one of them is a $D^*\bar{D}^*$ loosely bound state with quantum numbers $J^{PC} = 2^{++}$ [18,19]. The recent study of the production cross section of the $X(3872)$ relative to the $\psi(2S)$ in pp collisions by LHCb shows that the $X(3872)$ production is less suppressed relative to the prompt $\psi(2S)$ in the higher p_T region [20], which is similar to the case of $\psi(2S)$ relative to J/ψ [21,22]. Belle found evidence for $X(3872)$ production in two-photon collisions [23], thus motivating the search for the possible 2^{++} partner of the $X(3872)$ in such collisions. Such a study can provide essential information to understand the nature of the $X(3872)$.

Concurrently, there have been many studies related to the $\chi_{cJ}(2P)$ triplet states. The $Z(3930)$ was discovered by

Belle in the process $\gamma\gamma \to D\bar{D}$, and the angular distribution was used to identify it as the $\chi_{c2}(2P)$ state [4]. The existence of $Z(3930)$ and its angular distribution were confirmed by *BABAR* [5]. The $X(3915)$ was discovered by Belle [7] and a spin-parity analysis of this state by *BABAR* favored the $J^{PC} = 0^{++}$ quantum numbers [8]. The $X(3915)$ is a candidate of the $\chi_{c0}(2P)$ state [24–27]. In a recent amplitude analysis of the $B^+ \to K^+D^+D^-$ decay by LHCb [28], there are both 0^{++} and 2^{++} states at $m(D^+D^-) \approx 3930\ \mathrm{MeV}/c^2$. Their parameters are determined to be $M = 3923.8 \pm 1.5 \pm 0.4\ \mathrm{MeV}/c^2$ and $\Gamma = 17.4 \pm 5.1 \pm 0.8$ MeV for $\chi_{c0}(3930)$ and $M = 3926.8 \pm 2.4 \pm 0.8\ \mathrm{MeV}/c^2$ and $\Gamma = 34.2 \pm 6.6 \pm 1.1$ MeV for $\chi_{c2}(3930)$. (Here and hereafter, the first errors are statistical and the second are systematic.) The $\chi_{c2}(3930)$ state is a good candidate of $\chi_{c2}(2P)$, but this would imply that the hyperfine splitting of $12\ \mathrm{MeV}/c^2$ between $\chi_{c2}(2P)$ and $X(3915)$ would be only 6% of that between $\chi_{c2}(1P)$ and $\chi_{c0}(1P)$ [29]. In contrast, an early calculation [30] utilizing the Godfrey-Isgur relativistic potential model [31] predicts a much larger mass difference of about $60\ \mathrm{MeV}/c^2$ [30]. The $X^*(3860)$ observed by Belle is another candidate of $\chi_{c0}(2P)$ but it was not seen in LHCb's study of the $B^+ \to K^+D^+D^-$ decay [28]. One interpretation of the $X^*(3860)$ is a $D\bar{D}$ bound state close to the threshold with isospin $I = 0$ [32]. Therefore, additional studies of the P-wave triplet states near $3.9\ \mathrm{GeV}/c^2$ are needed for a more comprehensive understanding of the XYZ states and, in particular, of the $X(3872)$.

Both 0^{++} and 2^{++} states can be produced in two-photon collisions and can decay to $\gamma\psi(2S)$ via an E1 transition. For example, the partial widths are expected to be $\Gamma(\chi_{c0}(2P) \to \gamma\psi(2S)) \approx 135$ keV and $\Gamma(\chi_{c2}(2P) \to \gamma\psi(2S)) \approx 207$ keV according to the aforementioned calculation [30]. In this article, we report an investigation of the $\gamma\psi(2S)$ final state produced in two-photon collisions [$e^+e^- \to e^+e^-\gamma\gamma \to e^+e^-\gamma\psi(2S)$ or $\gamma\gamma \to \gamma\psi(2S)$ for brevity], using data collected with the Belle detector [33] at the KEKB asymmetric-energy e^+e^- collider [34]. The $\psi(2S)$ is reconstructed from its hadronic final state $\pi^+\pi^- J/\psi$ with J/ψ reconstructed from a lepton pair $\ell^+\ell^-(\ell = e, \mu)$.

II. DETECTOR, DATA SAMPLE, AND MONTE CARLO (MC) SIMULATION

The Belle detector is a large-solid-angle magnetic spectrometer that consists of a silicon vertex detector, a 50-layer central drift chamber, an array of aerogel threshold Cherenkov counters, a barrel-like arrangement of time-of-flight scintillation counters, and an electromagnetic calorimeter (ECL) comprised of CsI(Tl) crystals located inside a superconducting solenoid coil that provides a 1.5 T magnetic field. An iron flux return located outside of the coil is instrumented to detect K_L^0 mesons and to identify muons. The origin of the coordinate system is defined as the position of the nominal interaction point (IP). The z axis is aligned with the direction opposite the e^+ beam and is parallel to the direction of the magnetic field within the solenoid. The x axis is horizontal and points toward the outside of the storage ring; the y axis is vertical upward. The polar angle θ and azimuthal angle ϕ are measured relative to the positive z and x axes, respectively.

The integrated luminosity of Belle data used in this analysis is 980 fb^{-1}. About 70% of the data are collected at the $\Upsilon(4S)$ resonance, and the rest are taken at other $\Upsilon(nS)$ ($n = 1, 2, 3$, or 5) states or center-of-mass (c.m.) energies a few tens of MeV below the Υ states. The TREPS event generator [35] is used to simulate the signals of $\gamma\gamma \to X \to \gamma\psi(2S)$ for optimization of selection criteria, efficiency determination and calculation of the luminosity function $L_{\gamma\gamma}$ of two-photon collisions in Belle data. Here, X is $\chi_{c2}(3930)$, $X(3915)$ or a resonance with mass fixed to a value between 3.8 and $4.2\ \mathrm{GeV}/c^2$ and width fixed to zero. In the production of $\gamma\gamma \to X$, the helicity λ is the direction of the $\gamma\gamma$ axis in the rest frame of X. The $|\lambda| = 2$ component is reported to dominate in the measurements of $\gamma\gamma \to \chi_{c2}(3930) \to D\bar{D}$ by Belle [4] and *BABAR* [5]. A sample of $\chi_{c2}(3930)$ with helicity $|\lambda| = 2$ is taken to be the nominal signal MC sample. The major background is found to be the initial-state radiation (ISR) process $e^+e^- \to \psi(2S)$, which has a cross section of $15.42 \pm 0.12 \pm 0.89$ fb in the Belle data sample [36]. There are 0.6×10^6 events with a $\pi^+\pi^-\ell^+\ell^-$ final state in data, and an MC sample containing 3.8×10^6 such events is simulated with the PHOKHARA generator, which has a precision better than 0.5% [37]. An MC simulation using GEANT3 [38] is used to model the performance of the Belle detector.

III. SELECTION CRITERIA AND SIGNAL RECONSTRUCTIONS

Photon candidates are reconstructed from ECL clusters that do not match any charged tracks; the candidate with the highest energy is selected to form the $\gamma\psi(2S)$ final state. This energy is required to be larger than 100 MeV to suppress the background from fake photons. A candidate of $\psi(2S) \to \pi^+\pi^- J/\psi$ with $J/\psi \to e^+e^-$ or $\mu^+\mu^-$ is reconstructed from four well-measured charged tracks, each having impact parameters with respect to the IP of $|dz| < 5$ cm along the z (positron-beam) axis and $dr < 0.5$ cm in the transverse r-ϕ plane. For a charged track, information from the detector subsystems is combined to form a likelihood $\mathcal{L}_i$ for a particle species of $i \in \{e, \mu, \pi, K \text{ or proton}\}$ [39]. Tracks with $\mathcal{R}_K = \mathcal{L}_K/(\mathcal{L}_K + \mathcal{L}_\pi) < 0.4$ are identified as pions with an efficiency of about 95%, while 6% of kaons misidentified as pions. Similar likelihood ratios are formed for electron and muon identification [40,41]. Both lepton candidates are required to have $\mathcal{R}_e > 0.1$ for the $J/\psi \to e^+e^-$ mode; at least one candidate is required to have $\mathcal{R}_\mu > 0.1$ for the $J/\psi \to \mu^+\mu^-$ mode. For the first mode, any bremsstrahlung

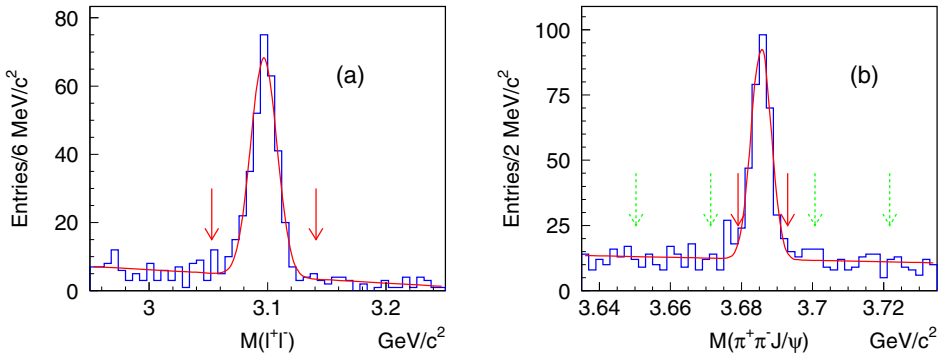

FIG. 1. Invariant mass distributions of (a) $\ell^+\ell^-(l = e, \mu)$ for the J/ψ signal and (b) $\pi^+\pi^- J/\psi$ for the $\psi(2S)$ signal in data. The curves show the best fit results. The red solid arrows show the signal regions and the green dashed arrows show the sideband regions.

photons detected in the ECL within 0.05 radians of the original lepton direction are included in the calculation of the e^+e^- invariant mass.

The invariant mass distributions of the lepton pair ($M_{\ell^+\ell^-}$) from data are shown in Fig. 1(a), where clear J/ψ signals are seen. By fitting the $M_{\ell^+\ell^-}$ distributions with a Gaussian function for the J/ψ signal and a first-order polynomial function for background, we obtain the J/ψ mass resolutions of 11.0 ± 0.6 MeV/c^2 from data and 9.4 ± 0.1 MeV/c^2 from signal MC simulation. A lepton pair is regarded as a J/ψ candidate if $|M_{\ell^+\ell^-} - m_{J/\psi}| < 4\sigma_{J/\psi}$, where $\sigma_{J/\psi} \equiv 11.0$ MeV/c^2 is taken from the resolution in data and $m_{J/\psi}$ is the nominal mass of J/ψ [1]. Figure 1(b) shows the distributions of $M_{\pi^+\pi^- J/\psi} \equiv M_{\pi^+\pi^-\ell^+\ell^-} - M_{\ell^+\ell^-} + m_{J/\psi}$ from data, where $M_{\pi^+\pi^-\ell^+\ell^-}$ is the invariant mass of $\pi^+\pi^-\ell^+\ell^-$. Fitting the $M_{\pi^+\pi^- J/\psi}$ distributions with a Gaussian function for $\psi(2S)$ signal and a first-order polynomial function for the background, we obtain the $\psi(2S)$ mass resolutions of 2.80 ± 0.21 MeV/c^2 from data and 2.52 ± 0.04 MeV/c^2 from the signal MC simulation. The $\psi(2S)$ signal window is defined to be $|M_{\pi^+\pi^- J/\psi} - m_{\psi(2S)}| < 2.5\sigma_{\psi(2S)}$, where $\sigma_{\psi(2S)} \equiv 2.8$ MeV/c^2 is taken from the resolution in data and $m_{\psi(2S)}$ is the nominal mass of $\psi(2S)$ [1]. To estimate the background in the $\psi(2S)$ reconstruction, the sideband regions are defined to be $|M_{\pi^+\pi^- J/\psi} - m_{\psi(2S)} \pm 9\sigma_{\psi(2S)}| < 3.75\sigma_{\psi(2S)}$, which are 3 times the width of the signal region.

The background is dominated by $e^+e^- \to \psi(2S)$ via ISR, where $\psi(2S)$ is combined with a fake photon. Figure 2 shows the distributions of the recoil mass squared $M^2_{\rm rec}(\gamma\psi(2S))$ of $\gamma\psi(2S)$. For two-photon collision events, there may be an outgoing e^+e^- pair traveling back-to-back along the e^+e^- beams so that $M^2_{\rm rec}(\gamma\psi(2S))$, corresponding to the mass squared of the outgoing e^+e^- pair, tends to be large. For ISR events, the recoil of $\gamma\psi(2S)$ is dominated by one energetic ISR photon with $E(\gamma_{\rm ISR}) > 1.5$ GeV, so $M^2_{\rm rec}(\gamma\psi(2S))$ is around zero. We apply $M^2_{\rm rec}(\gamma\psi(2S)) > 10$ (GeV/c^2)^2 to remove most ISR events. Nevertheless, there still remain events with two ISR photons traveling back-to-back along the e^+e^- collision beams; such events have a topology similar to two-photon collisions.

To suppress the ISR background further, the transverse momenta of $\psi(2S)$ and $\gamma\psi(2S)$, i.e., $P_t^*(\psi(2S))$ and $P_t^*(\gamma\psi(2S))$, calculated in the c.m. system and shown in Figs. 3(a) and 3(c), are used. $P_t^*(\gamma\psi(2S))$ is small for most of the signal events, in which the outgoing e^+e^- travel along the accelerator beamline. However, $P_t^*(\psi(2S))$ could be large if $\psi(2S)$ originates from the decay of a resonance such as $\chi_{c0}(2P)$ or $\chi_{c2}(2P)$. For the ISR events, $P_t^*(\psi(2S))$ is small since the ISR photon(s) always travel along the accelerator beamline. We optimize the selections of $P_t^*(\psi(2S))$ and $P_t^*(\gamma\psi(2S))$ based on the Punzi figure of merit (FOM), defined as

$$\text{FOM} \equiv \frac{\varepsilon(t)}{a/2 + \sqrt{N_{\rm bkg}(t)}} \tag{1}$$

according to Eq. (7) of Ref. [42]. Here, $\varepsilon(t)$ is the signal efficiency based on the selection criterion t, a is the number

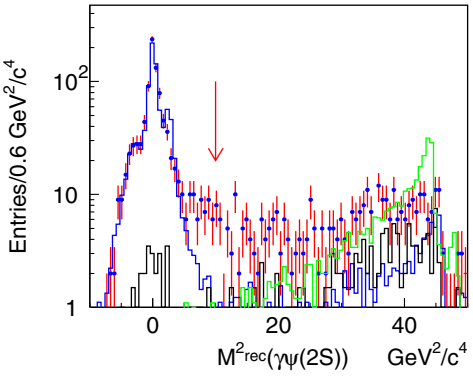

FIG. 2. The distributions of recoil mass square of $\gamma\psi(2S)$. The dots with error bars are data, the black blank histogram is the background estimated from the $\psi(2S)$ mass sidebands, the blue histogram is the ISR MC simulation and the green histogram is the signal MC simulation. The normalization of ISR MC simulation is according to the region $M^2_{\rm rec}(\gamma\psi(2S)) < 10$ (GeV/c^2)^2, and the one of the signal MC simulation is arbitrary. The arrow shows the position of $M^2_{\rm rec}(\gamma\psi(2S)) = 10$ (GeV/c^2)^2.

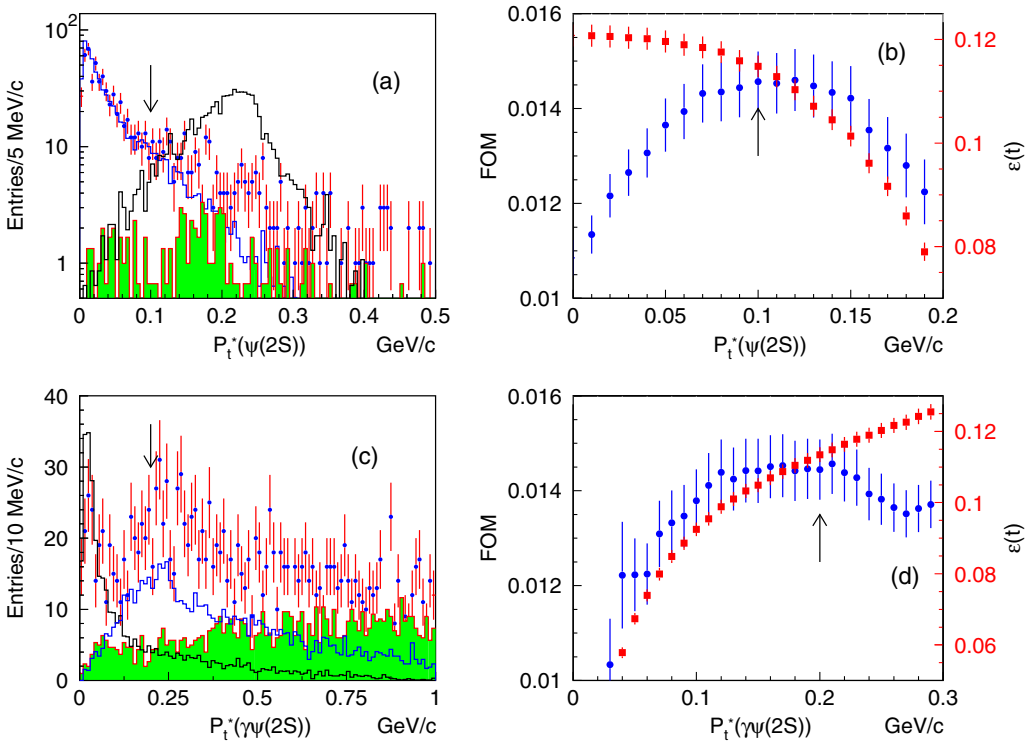

FIG. 3. The distributions of transverse momenta of $\psi(2S)$ (top row) and $\gamma\psi(2S)$ (bottom row) in the c.m. system of e^+e^- collision. In the left panel, the dots with error bars are from the signal region, the shaded histograms are the backgrounds estimated from the $\psi(2S)$ mass sidebands, the black blank histograms are signal MC simulation with arbitrary normalizations, and the blue blank histograms are ISR MC simulation. The normalization of the ISR MC simulation in (a) is according to data with $P_t^*(\psi(2S)) < 0.1$ GeV/c^2, and the one in (c) is according to the size of the ISR MC simulation sample. The right panel shows the Punzi FOMs in dots and efficiencies in diamonds versus (b) $P_t^*(\psi(2S))$ and (d) $P_t^*(\gamma\psi(2S))$. The arrows show the selections applied.

of sigmas corresponding to one-side Gaussian tests—we take $a = 5$—and $N_{\rm bkg}(t)$ is the background estimated from the ISR events and the $\psi(2S)$ mass sidebands. We do the optimization on $P_t^*(\psi(2S))$ and $P_t^*(\gamma\psi(2S))$ individually and iterate the procedure until both selections are at their optimal values. The FOM and $\varepsilon(t)$ versus P_t^* selections are shown in Figs. 3(b) and 3(d). We apply $P_t^*(\psi(2S)) > 0.1$ and $P_t^*(\gamma\psi(2S)) < 0.2$ GeV/c with selection efficiencies of $\varepsilon^{\rm MC}(t) = (97.1 \pm 0.3)\%$ and $\varepsilon^{\rm MC}(t) = (67.8 \pm 0.7)\%$, respectively. There are about 150 ISR events surviving these selection criteria with an efficiency of about 0.02%.

IV. INVARIANT MASS DISTRIBUTION OF $\gamma\psi(2S)$ AND TWO STRUCTURES

Figure 4 shows the invariant mass distributions for data of $\gamma\psi(2S)$ ($M_{\gamma\psi(2S)}$) in the $J/\psi \to e^+e^-$ and $\mu^+\mu^-$ modes [43]. The distributions of the backgrounds estimated from

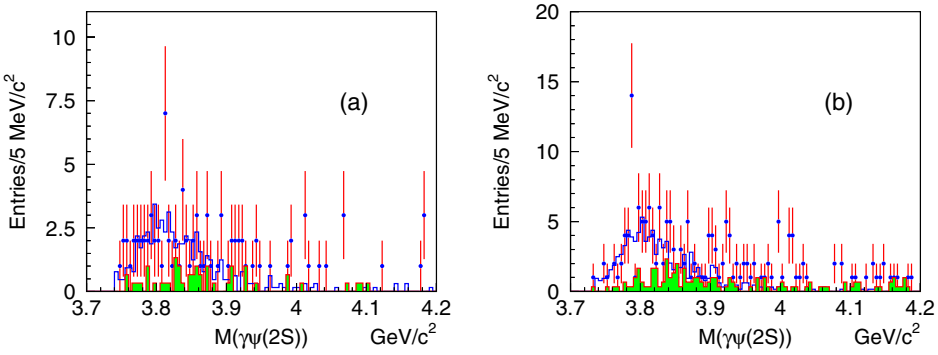

FIG. 4. The invariant mass distributions of $\gamma\psi(2S)$ from (a) e^+e^- mode and (b) $\mu^+\mu^-$ mode. The dots with error bars are data, and the shaded histograms are backgrounds estimated from the $\psi(2S)$ mass sidebands. The blank histograms are ISR events simulated and scaled to the size of the Belle data sample.

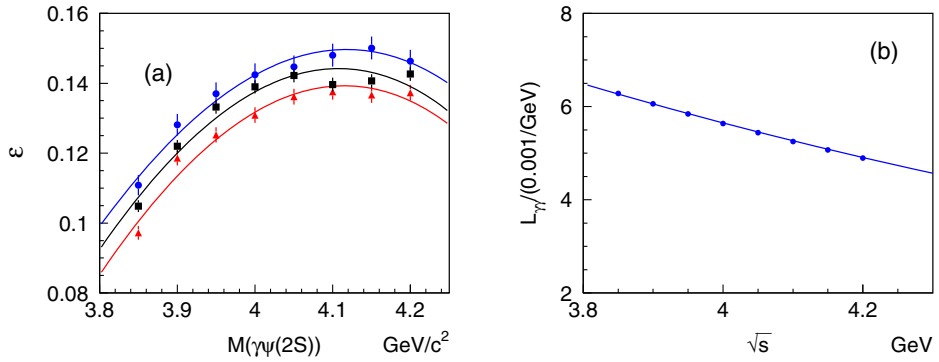

FIG. 5. (a) The efficiencies at different $M_{\gamma\psi(2S)}$ from MC simulation, and (b) the two-photon luminosity function $L_{\gamma\gamma}(\sqrt{s})$. In (a), the blue dots are the efficiencies for $J^{PC} = 0^{++}$, and the black (red) dots are the efficiencies for 2^{++} with helicity $|\lambda| = 0$ ($|\lambda| = 2$). The curves show the best fits with polynomial functions.

the scaled $\psi(2S)$ mass sidebands and ISR events simulated by PHOKHARA [37] are also shown in Fig. 4. The ratio between data and ISR MC simulation is 0.147 ± 0.012 from the distributions in the region $M_{\gamma\psi(2S)} < 3.9$ GeV/c^2, while the expected ratio is 0.156 ± 0.009 according to the cross section and the size of the ISR MC sample. Figure 5 shows the signal selection efficiency and the two-photon luminosity function $L_{\gamma\gamma}(\sqrt{s})$, which is defined as the probability of a two-photon emission with $\gamma\gamma$ c.m. system energy $\sqrt{s}$ in the Belle experiment [35]. The efficiencies for $J^{PC} = 0^{++}$ and 2^{++} ($|\lambda| = 0$ or 2) range from ∼10% to ∼15% for $M_{\gamma\psi(2S)}$ between 3.85 and 4.20 GeV/c^2.

The $M_{\gamma\psi(2S)}$ distribution of data after combining the e^+e^- and $\mu^+\mu^-$ modes is shown in Fig. 6. Excesses around 3.92 and 4.02 GeV/c^2 are seen. Both $\chi_{c2}(3930)$ and

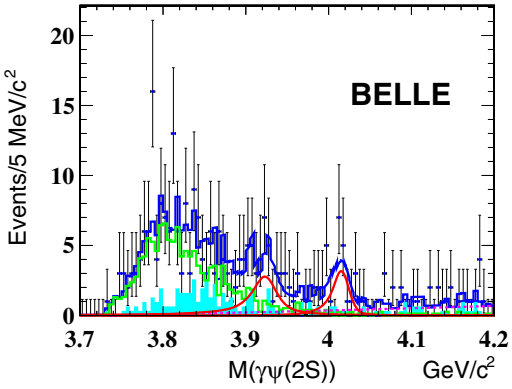

FIG. 6. The $\gamma\psi(2S)$ invariant mass distribution and the fit result. The points with error bars show the data while the shaded histogram is the normalized background from the $\psi(2S)$ mass sidebands. The solid blue curve shows the best fit results. The red signal curves from the convolutions of BW and CB functions show the contributions from the two structures. The green blank histogram shows the component of ISR events of $e^+e^- \to \psi(2S) \to \pi^+\pi^- J/\psi$. The pink dashed line shows the possible additional background, modeled by a second-order polynomial.

$X(3915)$ have the mass close to 3.92 GeV/c^2, but no resonance with a mass close 4.02 GeV/c^2 has been discovered in prior experiments. To study the excesses, a binned extended maximum-likelihood fit is performed to the $M_{\gamma\psi(2S)}$ mass spectra. The function used for the fit is characterized by the sum

$$f_{\rm sum} = f_{\rm R_1} + f_{\rm R_2} + f_{\rm ISR} + f_{\rm bkg} + f_{\rm SB}. \quad (2)$$

Here, $f_{\rm R_1}$ ($f_{\rm R_2}$) is for the structure R_1 (R_2) near 3.92 GeV/c^2 (4.02 GeV/c^2), $f_{\rm ISR}$ for the ISR events, $f_{\rm SB}$ for the background in $\psi(2S)$ reconstruction, and $f_{\rm bkg}$ for the possible additional backgrounds. The $f_{\rm SB}$ distribution is estimated from the $\psi(2S)$ mass sidebands, and its yield is fixed in the fits. Assuming the orbital angular momentum is zero between γ and $\psi(2S)$, the function $f_{\rm R_1}$ ($f_{\rm R_2}$) contains the convolution of a relativistic Breit-Wigner (BW) function with a form of $12\pi\Gamma_{\gamma\gamma}\Gamma_{\gamma\psi(2S)}/((s-M^2)^2 + M^2\Gamma^2)$ and a Crystal Ball (CB) function [44] with a mass resolution of about 7.4 MeV/c^2 (8.1 MeV/c^2), and the parameters of CB function are fixed according to the signal MC simulation of a resonance with a mass near that of the R_1 (R_2) state and with zero width. The resonant parameters in the BW function, viz. M, Γ, and $\Gamma_{\gamma\psi(2S)}$ ($\Gamma_{\gamma\gamma}$), are the mass, the width, and the partial width of the decay to the final state $\gamma\psi(2S)$ ($\gamma\gamma$), respectively. The product $\Gamma_{\gamma\psi(2S)}\Gamma_{\gamma\gamma}$ is treated as one parameter, since it is impossible to separate $\Gamma_{\gamma\psi(2S)}$ and $\Gamma_{\gamma\gamma}$ in the fits. The efficiency curve ε is shown in Fig. 5(a) and is incorporated into $f_{\rm R_1}$ and $f_{\rm R_2}$, i.e., $f_{\rm R} \propto \varepsilon({\rm BW} \otimes {\rm CB})$. The widths Γ_{R_1} and Γ_{R_2} are found to be small and thus the possible interference between R_1 and R_2 is expected to be small and is ignored in the fit. The histogram of $M_{\gamma\psi(2S)}$ distribution from the ISR MC simulation is used for $f_{\rm ISR}$. There may be more subdominant sources of background, such as high order QED processes and continuum production of $\gamma\gamma \to \gamma\psi(2S)$, but their individual and collective contributions are not clearly

TABLE I. Summary of the resonant parameters determined. The units of mass (M), width (Γ), product of partial width and branching fraction $\Gamma_{\gamma\gamma}\mathcal{B}$ are MeV/c^2, MeV and eV, respectively. The first errors are statistical and the second are systematic.

Resonant parameters	$J=0$	$J=2$
M_{R_1}	$3922.4 \pm 6.5 \pm 2.0$	
Γ_{R_1}	$22 \pm 17 \pm 4$	
$\Gamma_{\gamma\gamma}\mathcal{B}(R_1 \to \gamma\psi(2S))$	$9.8 \pm 3.6 \pm 1.3$	$2.0 \pm 0.7 \pm 0.2$
M_{R_2}	$4014.3 \pm 4.0 \pm 1.5$	
Γ_{R_2}	$4 \pm 11 \pm 6$	
$\Gamma_{\gamma\gamma}\mathcal{B}(R_2 \to \gamma\psi(2S))$	$6.2 \pm 2.2 \pm 0.8$	$1.2 \pm 0.4 \pm 0.2$

distinguishable with the current limited statistics. A second-order polynomial function is used for $f_{\rm bkg}$, and polynomial functions with different order are considered to estimate the systematic uncertainty.

The result from a fit in which all parameters are floated except the yield of the $f_{\rm SB}$ component is shown Fig. 6 and Table I. The reduced chi squared of the fit to the $M_{\gamma\psi(2S)}$ spectrum is $\chi^2/ndf = 0.69$. The signal yields are $N_{R_1} = 31 \pm 11$ events for R_1 with $M_{R_1} = 3922.4 \pm 6.5$ MeV/c^2 and $\Gamma_{R_1} = 22 \pm 17$ MeV, and $N_{R_2} = 19 \pm 7$ events for R_2 with $M_{R_2} = 4014.3 \pm 4.0$ MeV/c^2 and $\Gamma_{R_2} = 4 \pm 11$ MeV.

The production of R_1 and R_2 in two-photon collisions is studied by determining the parameter $\mathcal{B}\cdot\Gamma_{\gamma\gamma} \equiv \Gamma_{\gamma\psi(2S)}\Gamma_{\gamma\gamma}/\Gamma$ with the formula [35]

$$\mathcal{B}\cdot\Gamma_{\gamma\gamma} = \frac{n_{\rm fit}^{\rm sig}}{L_{\rm tot}\cdot\mathcal{B}^{\rm prod}\cdot\varepsilon\cdot F(\sqrt{s},J)}, \tag{3}$$

where $n_{\rm fit}^{\rm sig}$ is the signal yield from the fit, $L_{\rm tot} = 980$ fb^{-1} is the integrated luminosity of the Belle data sample, J is the spin of a structure, and $\mathcal{B}^{\rm prod}$ is the product of branching fractions $\mathcal{B}(\psi(2S) \to \pi^+\pi^- J/\psi)\cdot\mathcal{B}(J/\psi \to e^+e^-/\mu^+\mu^-)$. Since Γ_{R_1} and Γ_{R_2} are small compared to the available kinetic energy in the decays, the spin-dependent factor is $F(\sqrt{s},J) = 4\pi^2(2J+1)L_{\gamma\gamma}(\sqrt{s})/s$. The best fit gives $\Gamma_{\gamma\gamma}\mathcal{B}(R_1 \to \gamma\psi(2S)) = (9.8 \pm 3.6)$ eV if $J=0$ and (2.0 ± 0.7) eV if $J=2$ for structure R_1, and $\Gamma_{\gamma\gamma}\mathcal{B}(R_2 \to \gamma\psi(2S)) = (6.8 \pm 2.8)$ eV if $J=0$ and (1.4 ± 0.6) eV if $J=2$ for structure R_2. The ISR yield of 134 ± 15 is consistent with the estimate from the ISR MC simulation of 154 ± 10. The mass of R_1 indicates that it is a good candidate for $X(3915)$, $\chi_{c2}(3930)$ or an admixture of them. An alternate fit with both structures included and M_{R_1} and Γ_{R_1} fixed to the nominal $X(3915)$ parameters yields $\Gamma_{\gamma\gamma}\mathcal{B}(X(3915) \to \gamma\psi(2S)) = 9.6 \pm 2.9 \pm 1.1$ eV if $J^{PC} = 0^{++}$ and $1.9 \pm 0.6 \pm 0.2$ eV if $J^{PC} = 2^{++}$. Another alternative fit with the mass and width of R_1 fixed to those of $\chi_{c2}(3930)$ yields $\Gamma_{\gamma\gamma}\mathcal{B}(\chi_{c2}(3930) \to \gamma\psi(2S)) = 2.2 \pm 0.6 \pm 0.4$ eV if $J^{PC} = 2^{++}$. A third alternate fit with R_1 being an admixture of $X(3915)$ and $\chi_{c2}(3930)$ shows no notable change in the fit quality. The systematic uncertainties here are described in Sec. V.

The local signal significance is determined to be 3.5σ for R_1 and 3.4σ for R_2 by comparing the value of $\Delta(-2\ln\mathcal{L}) = -2\ln(\mathcal{L}_{\rm max}/\mathcal{L}_0)$ and the change of the number of free parameters ($N_{\rm par}$) in the fits, where $\mathcal{L}_{\rm max}$ is the likelihood with both R_1 and R_2 included in Eq. (2), and $\mathcal{L}_0$ is the likelihood with only one of R_1 or R_2 excluded. The values of $-2\ln\mathcal{L}$, χ^2/ndf, and $N_{\rm par}$ of these fits are summarized in Table II. The local signal significance of R_1 is determined to be 4.1σ (3.9σ) in the case that its mass and width are fixed to those of $X(3915)$ ($\chi_{c2}(3930)$). Taking into account the systematic uncertainties, described in Sec. V, the lowest value of the local significance of R_1 is 3.1σ. Since R_2 has never been seen before, the look-elsewhere effect is assessed for it with pseudo-experiments to check its global significance. The function for generating pseudo-experiments is $f_{\rm toyMC} = f_{\rm R_1} + f_{\rm ISR} + f_{\rm bkg} + f_{\rm SB}$ with the parameters from the nominal fit. The fit in each pseudo-experiment is performed with the same procedures as for the nominal fit to the actual data sample, except that the mass range of R_2 is limited to $M_{R_2} > 3.95$ GeV/c^2 because the region $M_{\gamma\psi(2S)} < 3.95$ GeV/c^2 is dominated by R_1 and ISR backgrounds. Among the 5.0×10^4 pseudo-experiments, the number of experiments with $\Delta(-2\ln\mathcal{L})$ of R_2 signal larger than the one from data is 137. Therefore, the probability considering the look-elsewhere effect is about $(2.74 \pm 0.23) \times 10^{-3}$, corresponding to a global significance of 2.8σ. Since the mass of R_1 is close to that of $X(3915)$ or $\chi_{c2}(3930)$ and the width—with its large uncertainty—has no conflict with that of $X(3915)$ or

TABLE II. The values of $-2\ln\mathcal{L}$, χ^2/ndf and number of free parameters ($N_{\rm par}$) in the different fits. From left to right, the rows are the fits with no resonance included, only R_1 included, only R_2 included, both R_1 and R_2 included (nominal fit), both resonances included and the mass and width of R_1 fixed to those of $X(3915)$, and both resonances included and the mass and width of R_1 fixed to those of $\chi_{c2}(3930)$. Only the differences among $-2\ln\mathcal{L}$ are meaningful in studying the statistical significance of R_1 and R_2.

…	No resonance	R_1 only	R_2 only	$R_1 + R_2$	$X(3915) + R_2$	$\chi_{c2}(3930) + R_2$
$-2\ln\mathcal{L}$	−2932.2	−2946.5	−2946.3	−2965.4	−2964.8	−2963.0
χ^2/ndf	0.76	0.74	0.78	0.70	0.68	0.68
$N_{\rm par}$	5	8	8	11	9	9

$\chi_{c2}(3930)$, we do not treat R_1 as a new never-observed state and so the look-elsewhere effect study is not performed to it.

V. SYSTEMATIC UNCERTAINTIES

There are systematic uncertainties in determining the resonant parameters of the two structures. The masses and widths are determined from fitting to the invariant mass distribution of $\gamma\psi(2S)$. In determining $\mathcal{B}\cdot\Gamma_{\gamma\gamma}$ with Eq. (3), additional systematic uncertainties from the selection efficiency, the luminosity of Belle data sample and the branching fractions of J/ψ and $\psi(2S)$ decays are taken into account.

The uncertainties due to the fits are estimated by changing the fit range, the number and the $f_{\rm SB}$ shape of the background in the $\psi(2S)$ reconstruction, the $f_{\rm bkg}$ shape, the bin width of the $M_{\gamma\psi(2S)}$ distribution, the parametrization of the BW function, and the resonant parameters of $X(3915)$ and $\chi_{c2}(3930)$. The fit range is changed from $[3.70, 4.20]$ to $[3.725, 4.15]$ GeV/c^2. The number of $\psi(2S)$ mass sideband events is changed by 1σ, and the sideband region is changed from $|M_{\pi^+\pi^- J/\psi} - m_{\psi(2S)} \pm 9\sigma_{\psi(2S)}| < 3.75\sigma_{\psi(2S)}$ to $|M_{\pi^+\pi^- J/\psi} - m_{\psi(2S)} \pm 8\sigma_{\psi(2S)}| < 3.75\sigma_{\psi(2S)}$ to estimate the uncertainty due to the $f_{\rm SB}$ component. Another ISR MC sample is simulated to estimate the uncertainty from the shape of $f_{\rm ISR}$. The alternative polynomial function for $f_{\rm bkg}$ is first order or third order. The bin width is changed from 5 to 4 MeV/c^2. The alternative formula of the resonant shape is $\mathrm{BW} \propto (M^2/s)\cdot 12\pi\Gamma_{\gamma\gamma}\Gamma_X/((s-M^2)^2 + M^2\Gamma^2)$. The uncertainty from the resolution of $M_{\gamma\psi(2S)}$ is mainly related to the reconstructed γ, and it is estimated with a sample of about $4,000\gamma\gamma \to \chi_{c2} \to \gamma J/\psi$ events selected in the Belle data sample. Fitting to χ_{c2} signals in the $M_{\gamma J/\psi}$ distributions from data and MC simulation results in the consistent value of 10.84 ± 0.26 and 10.77 ± 0.22 MeV/c^2, respectively. Thus, the uncertainty due to the mass resolution of $\gamma\psi(2S)$ is expected to be very small and so is ignored. When M_{R_1} and Γ_{R_1} are fixed to those of $X(3915)$ or $\chi_{c2}(3930)$, their values are changed by 1σ to estimate the related systematic uncertainties [1]. The largest differences between the nominal fit results and those from these various fits are taken as the systematic uncertainties of the mass, the width and the product $\Gamma_{\gamma\gamma}\mathcal{B}(R \to \gamma\psi(2S))$. A fit bias study using 200 toy MC samples shows that the bias of N_{R_1} is less than 3%, and those of other parameters are negligible. The statistics of each toy MC sample is 500 times of data to avoid the large fluctuations in testing the fit procedure. We take 3% to be the systematic uncertainty due to the fit bias for N_{R_1}.

Several sources of non-fit-related systematic uncertainties are considered. The particle identification uncertainty is 2.8% [39–41]; the uncertainty of the tracking efficiency is 0.35% per track and is additive; the uncertainty of the photon reconstruction is 2% per photon. The efficiency for the tracks in the extreme forward and backward regions obtained from MC simulation is found to be higher than that obtained in data according to the study of $e^+e^- \to \psi(2S) \to \pi^+\pi^- J/\psi$ via ISR [36], and appropriate corrections have been applied. The uncertainty in the $\psi(2S)$ mass window requirement is measured to be 0.6%, while the one of the J/ψ mass window is ignored. The efficiencies of the selection criteria on $P_t^*(\psi(2S))$ and $P_t^*(\gamma\psi(2S))$ are strongly related to the boost transformation from the lab system to the c.m. system of e^+e^- collisions. However, the related uncertainty is very small, and 1% is taken to be a conservative estimation for the uncertainty due to the P_t^* selections. The uncertainty due to the $M^2_{\rm rec}(\gamma\psi(2S))$ requirement is less than 0.5%. The uncertainty due to the momentum and angular distributions of helicities 0 and 2 for $J = 2$ is estimated to be 4.3% from the TREPS generator [35], while the one of $J = 0$ is ignored with the decay to $\gamma\psi(2S)$ isotropic and no uncertainty in helicity. The systematic uncertainty of the luminosity function from TREPS is 2.5%, which includes 1.1% from the calculation, under 1.0% from the form factor and 1%–2% from the radiative-correction effect [45]. Belle measures the luminosity with 1.4% precision. The trigger efficiency for the events surviving the selection criteria exceeds 99.4%, and so the uncertainty is ignored. The uncertainties of the J/ψ and $\psi(2S)$ decay branching fractions taken from Ref. [1] contribute a systematic uncertainty of 1.3%. The statistical error in the MC determination of the efficiency is less than 0.7%.

The non-fit-related systematic uncertainties are listed in Table III. Assuming all the sources are independent, we add them in quadrature to obtain a total systematic uncertainty of 6.6% (5.1%) of $J = 2$ ($J = 0$) in determining $\mathcal{B}\cdot\Gamma_{\gamma\gamma}$, in addition to the uncertainties from the fits.

TABLE III. The summary of systematic uncertainties besides the fits in $\gamma\gamma \to \gamma\psi(2S)$ measurement.

Source	Relative error (%)	
…	$J = 0$	$J = 2$
Particle identification	2.8	
Tracking efficiency	1.4	
Photon reconstruction	2.0	
$\psi(2S)$ mass window	0.6	
$P_t^*(\psi(2S))$ and $P_t^*(\gamma\psi(2S))$	1.0	
$M^2_{\rm rec}(\gamma\psi(2S))$	0.5	
Integrated luminosity	1.4	
Helicity	…	4.3
Luminosity function	2.5	
Branching fractions	1.3	
Statistics of MC samples	0.7	
Sum in quadrature	5.1	6.6

VI. DISCUSSION ON THE TWO STRUCTURES

We find evidence for the structure R_1 near 3.92 GeV/c^2, which may be $X(3915)$, $\chi_{c2}(3930)$, or an admixture of them. Assuming R_1 is $\chi_{c2}(3930)$ and taking into account $\Gamma_{\gamma\gamma}\mathcal{B}(\chi_{c2}(3930) \to D\bar{D}) = 210 \pm 40$ eV, the ratio $R = \mathcal{B}(\chi_{c2}(3930) \to \gamma\psi(2S))/\mathcal{B}(\chi_{c2}(3930) \to D\bar{D}) = 0.010 \pm 0.003$ is obtained. A rough estimation shows the partial width $\Gamma(\chi_{c2}(3930) \to \gamma\psi(2S)) = (200 \sim 300)$ keV, which is close to the predicted value of 207 keV from the Godfrey-Isgur relativistic potential model [30].

It is interesting to see that the mass of R_2 agrees with the HQSS-predicted mass ($\approx$4013 MeV/c^2) of the 2^{++} partner of $X(3872)$ [18]. The mass difference between R_2 and $X(3872)$ is 142.6 ± 4.2 MeV/c^2, while that between $D^{*0}(2007)$ and D^0 is 142.01 MeV/c^2. Meanwhile, the width of R_2 from the fit coincides with the predicted width of 2–8 MeV/c^2 for the 2^{++} partner of $X(3872)$ [19]. Thus, R_2 may provide important information for understanding the nature of the $X(3872)$. However, the global significance of R_2 is only 2.8σ. A much larger data sample that will be collected by Belle II may resolve this in the near future.

VII. SUMMARY

The two-photon process $\gamma\gamma \to \gamma\psi(2S)$ is studied in the $\gamma\gamma$ mass range from the threshold to 4.2 GeV/c^2 for the first time with the full Belle data sample, and two structures are seen in the invariant mass distribution of $\gamma\psi(2S)$. The first has a mass of $M_{R_1} = 3922.4 \pm 6.5 \pm 2.0$ MeV/c^2 and a width of $\Gamma_{R_1} = 22 \pm 17 \pm 4$ MeV with a local statistical significance of 3.1σ when the systematic uncertainties are included. This is close to the mass of $X(3915)$ and $\chi_{c2}(3930)$. The second has a mass of $M_{R_2} = 4014.3 \pm 4.0 \pm 1.5$ MeV/c^2 and a width of $\Gamma_{R_2} = 4 \pm 11 \pm 6$ MeV, with a global statistical significance of 2.8σ. The values of $\Gamma_{\gamma\gamma}\mathcal{B}(R \to \gamma\psi(2S))$ are of the order of several eV.

ACKNOWLEDGMENTS

We thank the KEKB group for the excellent operation of the accelerator; the KEK cryogenics group for the efficient operation of the solenoid; and the KEK computer group, and the Pacific Northwest National Laboratory (PNNL) Environmental Molecular Sciences Laboratory (EMSL) computing group for strong computing support; and the National Institute of Informatics, and Science Information NETwork 5 (SINET5) for valuable network support. We acknowledge support from the Ministry of Education, Culture, Sports, Science, and Technology (MEXT) of Japan, the Japan Society for the Promotion of Science (JSPS), and the Tau-Lepton Physics Research Center of Nagoya University; the Australian Research Council including Grants No. DP180102629, No. DP170102389, No. DP170102204, No. DP150103061, and No. FT130100303; Austrian Federal Ministry of Education, Science and Research (FWF) and FWF Austrian Science Fund No. P 31361-N36; the National Natural Science Foundation of China under Contracts No. 11435013, No. 11475187, No. 11521505, No. 11575017, No. 11675166, No. 11705209, and No. 12175041; Key Research Program of Frontier Sciences, Chinese Academy of Sciences (CAS), Grant No. QYZDJ-SSW-SLH011; the CAS Center for Excellence in Particle Physics (CCEPP); the Shanghai Science and Technology Committee (STCSM) under Grant No. 19ZR1403000; the Ministry of Education, Youth and Sports of the Czech Republic under Contract No. LTT17020; Horizon 2020 ERC Advanced Grant No. 884719 and ERC Starting Grant No. 947006 "InterLeptons" (European Union); the Carl Zeiss Foundation, the Deutsche Forschungsgemeinschaft, the Excellence Cluster Universe, and the Volkswagen-Stiftung; the Department of Atomic Energy (Project Identification No. RTI 4002) and the Department of Science and Technology of India; the Istituto Nazionale di Fisica Nucleare of Italy; National Research Foundation (NRF) of Korea Grants No. 2016R1D1A1B01010135, No. 2016R1D1A1B02012900, No. 2018R1A2B3003643, No. 2018R1A6A1A06024970, No. 2018R1D1A1B-07047294, No. 2019K1A3A7A09033840, and No. 2019R1I1A3A01058933; Radiation Science Research Institute, Foreign Large-size Research Facility Application Supporting project, the Global Science Experimental Data Hub Center of the Korea Institute of Science and Technology Information and KREONET/GLORIAD; the Polish Ministry of Science and Higher Education and the National Science Center; the Ministry of Science and Higher Education of the Russian Federation, Agreement No. 14.W03.31.0026, and the HSE University Basic Research Program, Moscow; University of Tabuk research Grants S-1440-0321, S-0256-1438 and No. S-0280-1439 (Saudi Arabia); the Slovenian Research Agency Grants No. J1-9124 and No. P1-0135; Ikerbasque, Basque Foundation for Science, Spain; the Swiss National Science Foundation; the Ministry of Education and the Ministry of Science and Technology of Taiwan; and the United States Department of Energy and the National Science Foundation.

[1] P. A. Zyla *et al.* (Particle Data Group), Prog. Theor. Exp. Phys. **2020**, 083C01 (2020) and 2021 update.

[2] S. K. Choi *et al.* (Belle Collaboration), Phys. Rev. Lett. **91**, 262001 (2003).

[3] For some recent review, see S. L. Olsen, T. Skwarnichi, and D. Zieminska, Rev. Mod. Phys. **90**, 015003 2018; N. Brambilla, S. Eidelman, C. Hanhart, A. Nefediev, C.-P. Shen, C. E. Thomas, A. Vairo, and C.-Z. Yuan, Phys. Rep. **873**, 1 (2020).

[4] S. Uehara *et al.* (Belle Collaboration), Phys. Rev. Lett. **96**, 082003 (2006).

[5] B. Aubert *et al.* (*BABAR* Collaboration), Phys. Rev. D **81**, 092003 (2010).

[6] R. Aaij *et al.* (LHCb Collaboration), J. High Energy Phys. 07 (2019) 035.

[7] S. Uehara *et al.* (Belle Collaboration), Phys. Rev. Lett. **104**, 092001 (2010).

[8] J. P. Lees *et al.* (*BABAR* Collaboration), Phys. Rev. D **86**, 072002 (2012).

[9] K. Chilikin *et al.* (Belle Collaboration), Phys. Rev. D **95**, 112003 (2017).

[10] E. S. Swanson, Phys. Lett. B **598**, 197 2004; Phys. Rep. **429**, 243 (2006).

[11] V. M. Abazov *et al.* (D0 Collaboration), Phys. Rev. Lett. **93**, 162002 (2004).

[12] R. Aaij *et al.* (LHCb Collaboration), Eur. Phys. J. C **72**, 1972 (2012).

[13] S. Chatrchyan *et al.* (CMS Collaboration), J. High Energy Phys. 04 (2013) 154.

[14] M. Aaboud *et al.* (ATLAS Collaboration), J. High Energy Phys. 07 (2017) 117.

[15] R. Aaij *et al.* (LHCb Collaboration), Phys. Rev. Lett. **110**, 222001 (2013); Phys. Rev. D **92**, 11102(R) 2015.

[16] R. Aaij *et al.* (LHCb Collaboration), Nucl. Phys. **B886**, 665 (2014).

[17] R. Aaij *et al.* (LHCb Collaboration), Phys. Rev. D **102**, 092005 (2020).

[18] F. K. Guo, C. Hidalgo-Duque, J. Nieves, and M. P. Valderrama, Phys. Rev. D **88**, 054007 (2013).

[19] M. Albaladejo, F. K. Guo, C. Hidalgo-Duque, J. Nieves, and M. P. Valderrama, Eur. Phys. J. C **75**, 547 (2015).

[20] R. Aaij *et al.* (LHCb Collaboration), J. High Energy Phys. 01 (2018) 131.

[21] S. Chatrchyan *et al.* (CMS Collaboration), J. High Energy Phys. 02 (2012) 011.

[22] R. Aaij *et al.* (LHCb Collaboration), Eur. Phys. J. C **72**, 2100 (2012).

[23] Y. Teramoto *et al.* (Belle Collaboration), Phys. Rev. Lett. **126**, 122001 (2021).

[24] X. Liu, Z. G. Luo, and Z. F. Sun, Phys. Rev. Lett. **104**, 122001 (2010).

[25] D. Y. Chen, J. He, X. Liu, and T. Matsuki, Eur. Phys. J. C **72**, 2226 (2012).

[26] M. X. Duan, S. Q. Luo, X. Liu, and T. Matsuki, Phys. Rev. D **101**, 054029 (2020).

[27] M. X. Duan, J. Z. Wang, Y. S. Li, and X. Liu, Phys. Rev. D **104**, 034035 (2021).

[28] R. Aaij *et al.* (LHCb Collaboration), Phys. Rev. D **102**, 112003 (2020).

[29] F. K. Guo, C. Hanhart, G. Li, Ulf-G. Meissner, and Q. Zhao, Phys. Rev. D **83**, 034013 (2011).

[30] T. Barnes, S. Godfrey, and E. S. Swanson, Phys. Rev. D **72**, 054026 (2005).

[31] S. Godfrey and N. Isgur, Phys. Rev. D **32**, 189 (1985).

[32] E. Wang, H. S. Li, W. H. Liang, and E. Oset, Phys. Rev. D **103**, 054008 (2021).

[33] A. Abashian *et al.* (Belle Collaboration), Nucl. Instrum. Methods Phys. Res., Sect. A **479**, 117 (2002); also see Section II in J. Brodzicka *et al.*, Prog. Theor. Exp. Phys. **2012**, 4D001 (2012).

[34] S. Kurokawa and E. Kikutani, Nucl. Instrum. Methods Phys. Res., Sect. A **499**, 1 (2003), and other papers included in this Volume; T. Abe *et al.*, Prog. Theor. Exp. Phys. **2013**, 03A001 (2013), and references therein and other papers included in this volume.

[35] S. Uehara, arXiv:1310.0157.

[36] C. Z. Yuan *et al.* (Belle Collaboration), Phys. Rev. Lett. **99**, 182004 (2007); Z. Q. Liu *et al.* (Belle Collaboration), Phys. Rev. Lett. **110**, 252002 (2013).

[37] G. Rodrigo, H. Czyż, J. H. Kühn, and M. Szopa, Eur. Phys. J. C **24**, 71 (2002).For a review on the generator, see S. Actis *et al.*, Eur. Phys. J. C **66**, 585 (2010).

[38] R. Brun *et al.*, GEANT3.21, Report No. CERN DD/EE/84-1, 1984.

[39] E. Nakano, Nucl. Instrum. Methods Phys. Res., Sect. A **494**, 402 (2002).

[40] K. Hanagaki, H. Kakuno, H. Ikeda, T. Iijima, and T. Tsukamoto, Nucl. Instrum. Methods Phys. Res., Sect. A **485**, 490 (2002).

[41] A. Abashian *et al.*, Nucl. Instrum. Methods Phys. Res., Sect. A **491**, 69 (2002).

[42] G. Punzi, arXiv:physics/0308063v2.

[43] $M_{\gamma\psi(2S)} = M_{\gamma\pi^+\pi^-\ell^+\ell^-} - M_{\pi^+\pi^-\ell^+\ell^-} + m_{\psi(2S)}$ is used to cancel the mass resolution due to $\pi^+\pi^-$ and $\ell^+\ell^-$ in the $\gamma\psi(2S)$ invariant mass spectrum.

[44] M. Oreglia, A study of the reactions $\psi' \to \gamma\gamma\psi$, Ph.D thesis, SLAC, 1980.

[45] W. L. Van Neerven and J. A. Vermaseren, Nucl. Phys. **B238**, 73 (1984); F. A. Berends, P. H. Daverveldt, and R. Kleiss, Nucl. Phys. **B253**, 421 (1985).